IAC-20-C1.8.6

From Magnetic to Aerodynamic Passive Stabilization: Case of Transient Attitude Motion of TNS-0#2 Nanosatellite

Mikhail Ovchinnikov [a], Danil Ivanov[b]*, Oleg Pansyrnyi [c], Igor Fedorov [d], Oleg Khromov [f], Nikolay Yudanov [g], Artem Sergeev [h]

[a] *Keldysh Institute of Applied Mathematics, RAS, Miusskaya sq.4, Moscow, Russian Federation, 125047,* ovchinni@keldysh.ru
[b] *Keldysh Institute of Applied Mathematics, RAS, Miusskaya sq.4, Moscow, Russian Federation, 125047,* danilivanovs@gmail.com
[c] *JSC Russian Space Systems, Aviamotornaya st. 53, Moscow, Russian Federation, 111250,* pantsyrnyi@mail.ru
[d] *JSC Russian Space Systems, Aviamotornaya st. 53, Moscow, Russian Federation, 111250,* tm016@rniikp.ru
[e] *JSC Russian Space Systems, Aviamotornaya st. 53, Moscow, Russian Federation, 111250,* khromovoe@mail.ru
[f] *JSC Russian Space Systems, Aviamotornaya st. 53, Moscow, Russian Federation, 111250,* kolyan2606@mail.ru
[g] *JSC Russian Space Systems, Aviamotornaya st. 53, Moscow, Russian Federation, 111250,* vorchun@yandex.ru
* Corresponding Author

Abstract

Attitude motion reconstruction of the Technological NanoSatellite TNS-0 #2 during the last month of the mission is presented in the paper. The main feature of the TNS-0 nanosatellite series is to use the Globalstar communication system. During the motion in the dense layers of the upper atmosphere up to altitude of 156 km the measurements from the on-board sensors was transmitted via Globalstar. It allowed to process the measurements and find the passive attitude regimes of the satellite. Initially after the launch and damping of the initial angular rotation the satellite was in passive magnetic stabilization due to permanent magnet on-board the satellite. The TNS-0#2 magnet axis tracked the local geomagnetic field direction with accuracy of about 15 deg during almost 2 years of the mission. However, with orbit altitude decay the aerodynamic torque started to significantly influence the attitude motion and the satellite attitude pass from the passive magnetic motion regime via tumbling transient motion to the aerodynamic stabilization. In the aerodynamic stabilization regime the satellite dynamical axis track the direction of the incoming airflow due to shift of the center of pressure relative to the center of mass. The details on the transient attitude motion and its analysis are given in the paper.

Keywords: nanosatellite, attitude determination, passive magnetic stabilization, aerodynamic stabilization

1. Introduction

Passive attitude control systems are quite popular for nano-, pico-, femto-satellites due to strict limitations in terms of mass, size, cost and energy. These systems utilize natural magnetic, gravitational or aerodynamic torques to provide stabilization appropriate for the mission. The ratio between the values of these major environmental torques changes as the satellite orbit evolves. The paper studies the transient attitude motion using telemetry data from TNS-0#2 nanosatellite.

Technological NanoSatellite TNS-0 #2 developed by JSC Russian Space Systems was successfully launched on August 17, 2017 from the International Space Station during the spacewalk of the Russian cosmonauts. The mass of the satellite is 4.8 kg and the form-factor is hexagonal prism. The main feature of the TNS-0 nanosatellite series is the GlobalStar communication system. The TNS-0 satellites upload and download the telemetry and other information via GlobalStar antennas [1]. The satellite is equipped with the passive magnetic attitude system developed by the Keldysh Institute of Applied Mechanics of RAS. The system consists of a set of hysteresis rods for the initial angular velocity damping and a permanent magnet located along the axis of symmetry to stabilize the axis along the local geomagnetic field induction vector. Three-axis magnetometer and a set of sun sensors are installed onboard. Attitude motion is reconstructed using their measurements.

After the damping of the initial angular velocity after the launch the satellite achieved a passive magnetic stabilization. The longitudinal axis of the satellite was directed approximately along the local geomagnetic induction vector with deviation that does not exceed 12 degrees. This attitude was provided with the passive magnetic control system. However, due to the natural altitude decrease aerodynamic torque influence increased. The satellite has a relatively elongated geometry with significant displacement between the centers of mass and pressure. On August 10, 2019 the magnetic attitude changed to almost chaotic motion with high angular velocity. In about 2 weeks the aerodynamic stabilization was achieved, which maintained till the breakdown in the atmosphere on

September 6, 2019. During the breakdown the chaotic tumbling is observed.

Passive magnetic attitude control systems were widespread at the dawn of the space age. A number of papers on attitude dynamics of satellites equipped with magnetic dampers and permanents magnets are well-known [2–6]. However, these attitude systems have become popular again with the advent of small and nano-satellites due to strict limitations in terms of mass, size, cost and energy on these satellites. One can mention nanosatellites Munin (2000г.) [7], QuakeSat (2003г.) [8], CUTE-I XI-IV (2003г.) [9], EduSAT (2011 г.) [10], Delfi-C3 (2008г.) [11]. Particular interest in the development and use of passive attitude magnetic systems is shown by universities and small companies entering the market of space services.

The algorithms of attitude motion determination using on-board sensors measurements are well studied in the literature. There are two main approaches the real-time on-board motion estimation using recursive algorithms [12,13] and post-flight measurement processing for motion reconstruction. The first approach is commonly used for active attitude control systems, and the second is more suitable for motion estimation of satellites with passive attitude control systems. In this paper magnetometer measurements processing technique is used for TNS-0 #2 nanosatellite attitude motion reconstruction. The technique is similar to the one that used for motion determination of Photon and Bion series satellites [14–16]. It consists in finding such initial conditions for the equations of angular motion at which the minimum of the difference of the squares of magnetic field measurements and predicted measurements calculated using the model of the angular motion of the satellite is reached.

2. TNS-0 #2 description

TNS-0 #2 nanosatellite has a body in the shape of hexagonal prism with 26.4 cm height and 18.7 cm of diameter. The sides of the device are covered with solar panels. Globalstar antennas, a set of solar sensors and a radio link antenna are located on the upper side of the satellite. A handle is attached to the bottom of the prism, for which the astronaut keeps the satellite on launch during the spacewalk. The satellite is presented in Fig. 1.

The mass of satellite is 4.8 kg, its center of mass is located on the axis of geometric symmetry of the satellite body, as shown in Fig. 2. The elements of the inertia tensor in the reference frame located in the center of mass of the satellite have the following values:

$$J = \begin{bmatrix} 0.06153 & -0.00013 & -0.00033 \\ -0.00013 & 0.06669 & -0.00012 \\ -0.00033 & -0.00012 & 0.01287 \end{bmatrix} \text{kg} \cdot \text{m}^2.$$

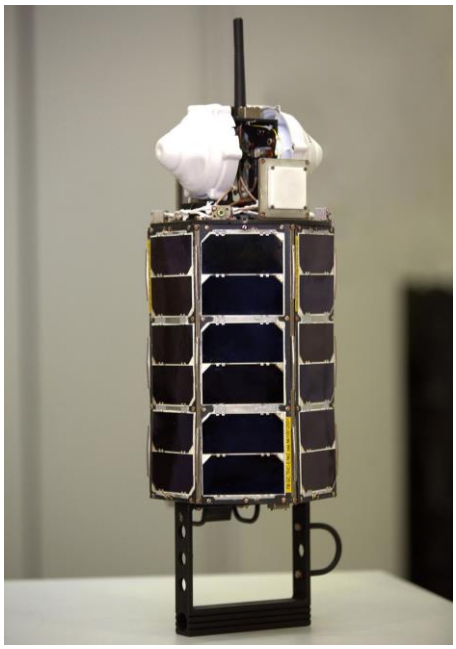

Fig. 1. The photo of the TNS-0 #2 nanosatellite

The value of the permanent magnet is equals to 2.2 $\text{A} \cdot \text{m}^2$. A grid of hysteresis rods is installed on the upper and lower sides of the nanosatellite body, they are used for damping the angular velocity after the launch. The location of the permanent magnet, as well as the magnetometer and solar sensors on the body of the satellite is shown in Fig. 2.

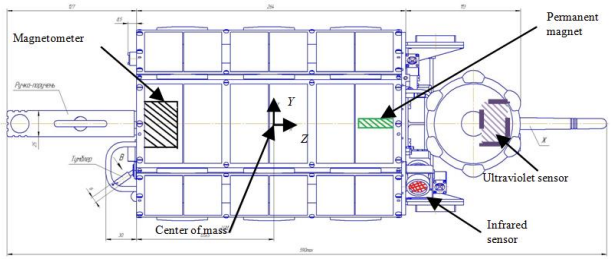

Fig.2. Center of mass location, permanent magnet, magnetometer and sun sensors position in the satellite body

The magnetometer installed on the satellite TNS-0 # 2 is designed for measuring the external magnetic field. The root-mean-square error of measurements of the magnetometer is $\sigma = 100$ nT. The non-orthogonality of the measuring axes is 1 degree. Eight optical sensors are installed on the nanosatellite THS-0 #2: six photodiode sensors, one ultraviolet solar sensor and one infrared horizon sensor.

More details on the passive attitude control system can be found in [17].

3. Attitude motion reconstruction technique

In this section, a technique for processing of the measurements from on-board sensors of the nanosatellite TNS-0 #2 for the angular motion reconstruction using the telemetry data is presented. A mathematical model of the angular motion of a nanosatellite with assumptions is written in details.

3.1 TNS-0#2 attitude motion equations

Consider the motion of a satellite with hysteresis rods fixed in its body and a permanent magnet taking into account the gravitational and magnetic torques. Assume that the satellite is a solid body moving along a circular orbit around the Earth. The SGP4 model is used to describe the gravitational field of the Earth. The geomagnetic field is described by the IGRF model. The parallelogram model is used to describe the effect of the hysteresis in rods [18].

To write the equations of motion of the satellite, we introduce two reference frames which are used to write the attitude motion equations. $OX_OY_OZ_O$ is the orbital reference frame with origin placed in the satellite center of mass. Axis OZ_O is directed along the satellite radius-vector, OY_O is perpendicular to the orbital plane, axis OX_O complements these axes; OXYZ is the body-fixed reference frame, its axes are directed as shown in Fig.2.

The attitude motion is described using dynamic Euler equations and kinematic relations based on the quaternions, elements of the matrix of direction cosines or Euler angles. The satellite state vector consists of the angular velocity vector and the selected set of angular variables. The quaternion $\Lambda = (\mathbf{q}, q_0)$ is used as the angular variable. Here $\mathbf{q}$ is the vector part of the quaternion and the q_0 is the scalar part. Also the direction cosine matrix $\mathbf{A}$ and Euler angles α, β, γ (rotation sequence 2-3-1) are used for the torques model formulae and for the attitude position representation correspondingly.

The dynamic equations are as follows:

$$\mathbf{J}\dot{\boldsymbol{\Omega}} + \boldsymbol{\Omega} \times \mathbf{J}\boldsymbol{\Omega} = \mathbf{M}_{mag} + \mathbf{M}_{grav} + \mathbf{M}_{hyst} + \mathbf{M}_{aero},$$

where $\mathbf{J}$ is inertia tensor, $\boldsymbol{\Omega}$ is absolute angular velocity, $\mathbf{M}_{mag}, \mathbf{M}_{grav}, \mathbf{M}_{hyst}$ are magnetic torques caused by permanent magnet, gravitational torque and magnetic torque due to hysteresis rods correspondingly. The gravitational torque is

$$\mathbf{M}_{grav} = 3\omega_0^2 (\mathbf{A}\mathbf{e}_3) \times \mathbf{J}(\mathbf{A}\mathbf{e}_3),$$

where $\mathbf{e}_3 = (0,\ 0,\ 1)^T$ is local vertical vector in the orbital reference frame, $\boldsymbol{\omega}_0$ is the orbital angular velocity vector, that has the following components in the orbital reference frame $\boldsymbol{\omega}_0 = [0 \quad \omega_0 \quad 0]^T$. The magnetic torque due to permanent magnet is as follows:

$$\mathbf{M}_{mag} = \mathbf{m} \times \mathbf{B},$$

where $\mathbf{m}$ is dipole magnetic moment of the permanent magnet, $\mathbf{B}$ is the vector of the Earth magnetic field. The torque caused by the hysteresis rods is

$$\mathbf{M}_{hyst} = \mathbf{m}_{hyst} \times \mathbf{B},$$

where $\mathbf{m}_{gist}$ is the resulting dipole magnetic moment of all the rods. For the magnetic moment of one rod one can write the following:

$$\mathbf{m}_{hyst}^k = \mu_k V_k H_0 W \mathbf{e}_k / \mu_0,$$

where μ_k is the relative magnetic permeability of the k-th rod, V_k is its volume, H_0 is the mean value of the geomagnetic field induction $\mathbf{H}$ in the current point of the orbit, $W(H_\tau)$ is dimensionless function describing dependence of the induction of the rod related to H_0 according to the parallelogram, μ_0 is the magnetic constant; $H_\tau = \mathbf{H}\mathbf{e}_k$, $\mathbf{e}_k$ is the unit vector directed along the rod in the body reference frame.

The aerodynamic torque is

The aerodynamic torque is

$$\mathbf{M}_{aero} = -\mathbf{d} \times \mathbf{f}_a.$$

Vector $\mathbf{d}$ determines the position of the satellite center of mass relative to the center of pressure, $\mathbf{f}_a$ is the aerodynamic drag force acting on the side in the body-fixed reference frame.

Dynamic equations are supplemented by kinematic relations. The quaternion is used in the numerical simulation of the attitude motion. Its kinematic equation is as follows

$$\dot{\Lambda} = \frac{1}{2}\mathbf{C}\Lambda,$$

$$\mathbf{C} = \begin{bmatrix} 0 & \omega_3 & -\omega_2 & \omega_1 \\ -\omega_3 & 0 & \omega_1 & \omega_2 \\ \omega_2 & -\omega_1 & 0 & \omega_3 \\ -\omega_1 & -\omega_2 & -\omega_3 & 0 \end{bmatrix}. \quad (1)$$

Here $\boldsymbol{\omega} = [\omega_1, \omega_2, \omega_3]^T$ is angular velocity relative the orbital reference frame, that is calculated using the formula

$$\boldsymbol{\omega} = \boldsymbol{\Omega} - \mathbf{A}\boldsymbol{\omega}_0.$$

3.2 Measurements processing technique

The problem of the attitude motion reconstruction is formulated as follows. It is necessary to obtain such initial conditions for the attitude motion equations that the difference between the predicted measurements calculated using measurement model and the actual measurements from the on-board sensor achieves a minimum by mean square criterion.

Consider an initial condition vector consisting of quaternion vector part $\mathbf{q}(t=0)$ and angular velocity vector $\boldsymbol{\omega}(t=0)$ at the initial time (the time of the first received telemetry with measurements):

$$\xi = \left[\mathbf{q}(t=0), \boldsymbol{\omega}(t=0)\right]^T .$$

If the vector ξ is defined, then one can calculate at each time t_k, when the measurements are available, the quaternion $\Lambda\left(t=t_k\right)$ obtained by the integration of the motion equations. Then one can predict the measurements for example of the magnetometer using the measurement model:

$$\tilde{\mathbf{b}}^k_{изм} = \mathbf{A}\left(\Lambda_k\right)\mathbf{b}^k_o ,$$

where the unit vector along the geomagnetic field in orbital reference frame $\mathbf{b}^k_o$ is calculated accordingly the orbital position of the satellite (obtained using either GPS/GLONASS receiver or by using TLE and SGP4 model) and geomagnetic model IGRF. Then the problem of the vector ξ determination reduces to the problem of the following function minimization

$$\Phi\left(\xi\right) = \sum_{k=1}^{N}\left(\left|\tilde{\mathbf{b}}^k_{\text{model}} - \mathbf{b}^k_{meas}\right|\right)^2 ,$$

where $\mathbf{b}^k_{meas}$ is the unit vector along the geomagnetic field calculated using measurements after excluding the constant bias. The minimization of the function $\Phi\left(\xi\right)$ is carried out using the nonlinear optimization methods.

4. Measurements processing results and passive attitude motion regimes analysis

4.1. Attitude stabilization after the launch

The first communication session, during which the telemetry with measurements of sensors was transmitted, was on August 19 at 17 hours 11 minutes UTC. In Fig. 3 shows the graph of measurements of the magnetometer and sun sensors that lasted for one minute.

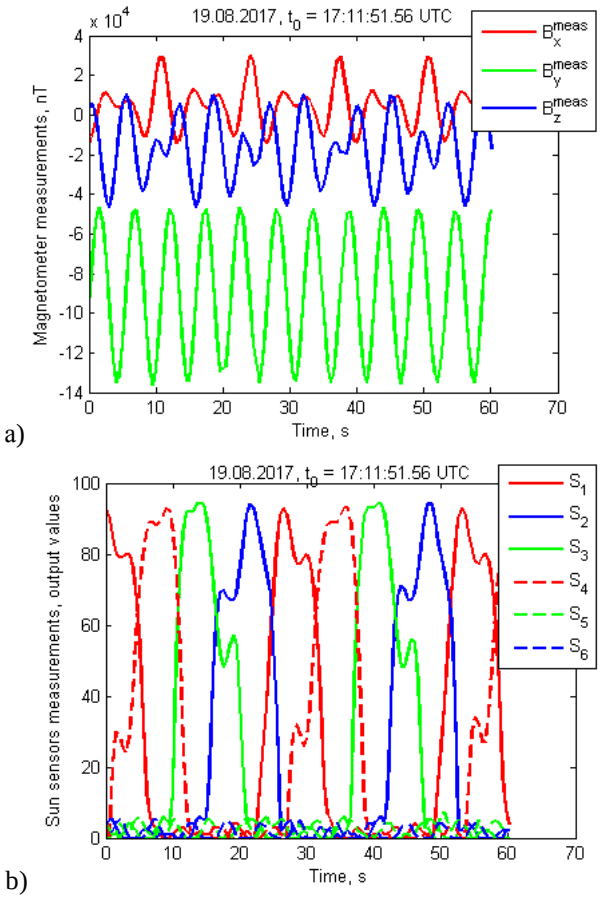

Fig. 3. First obtained measurements from magnetometer (a) and photodiode sensors (b)

In the measurements of the magnetometer, in addition to the geomagnetic field, there are components of constant bias due to the magnetic field of the permanent magnet (Fig. 2), as well as the variable components caused by magnetization of the hysteresis rods. To extract the measurements of the geomagnetic field, the contribution of the constant bias in the measurements was estimated using the least squares method. Fig. 4 shows a graph of the obtained Earth's magnetic field. The value of the constant bias of the magnetometer measurements is $\mathbf{B}_{bias} = \left[5.8 \quad -90.8 \quad -20.9\right]\cdot 10^3$ nT .

A unit vector along the geomagnetic field at the satellite location is calculated from the measurements obtained. Using the magnetic field model IGRF with the known position of the satellite at the time of the measurement, calculated using the TLE elements and the SGP4 motion model, a unit vector along the magnetic field in the orbital coordinate system is calculated.

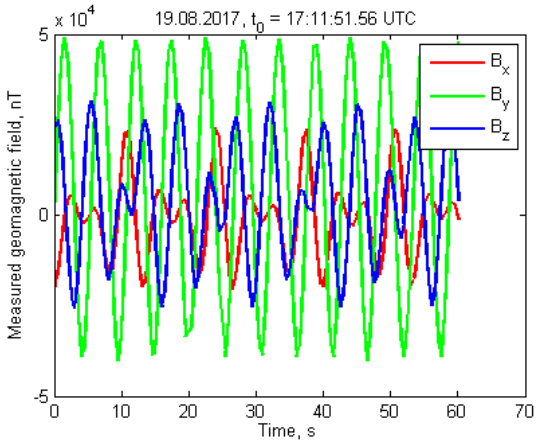

Fig.4. Measured geomagnetic field

Since the location of the magnetometer in the satellite body is known, then if one specifies the initial conditions for the angular motion, its measurement can be predicted. Thus, using the least squares method, we estimate a vector of initial conditions consisting of a quaternion and an angular velocity at the time of the measurement start, which minimizes the difference between the measured vectors along the geomagnetic field and its predicted motion model at each moment on a given telemetry segment. Fig. 5 depicts the graphs of the measured and predicted unit vector along the geomagnetic field. From this graph it can be concluded that the vector of the initial conditions close to the real one is found, since the values of the measurements and its prediction are close.

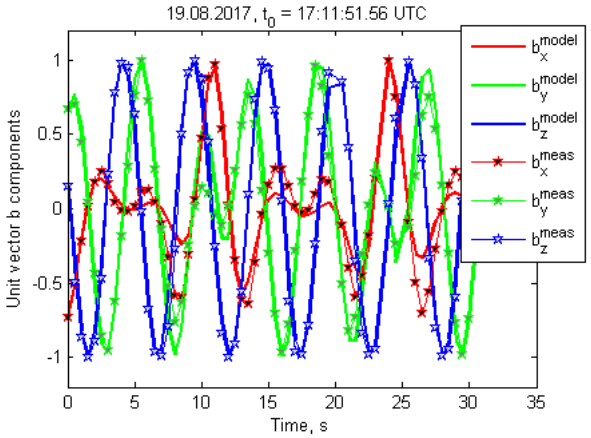

Fig. 5. Measured and predicted unit vector along the geomagnetic field

Fig. 6 shows the graphs of the quaternion calculated using the initial conditions obtained. Fig. 7 shows the angular velocity vector. Its value close to the one estimated using video of the launch processing.

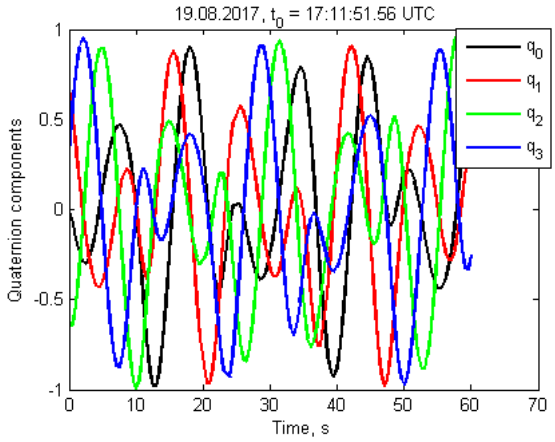

Fig. 6. Quaternion components

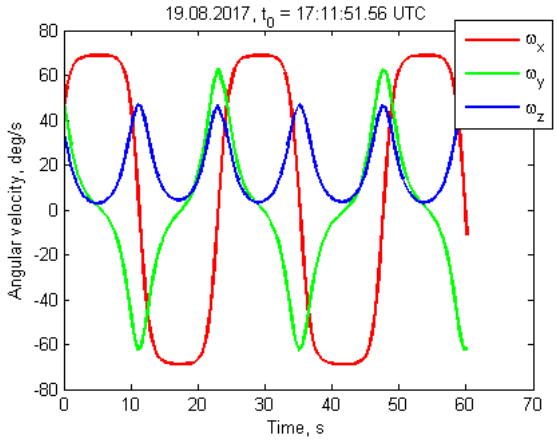

Fig. 7. Angular velocity components

To verify the obtained angular motion estimation, measurements from sun sensors were predicted and a comparison with actual measurements was made. It is assumed that the photodiode sensors have a sensitive area in the form of a cone with an angle of 120 degrees. The sensor measurements within this region is considered to have a cosine-like dependence on the incidence angle of the sun's rays, and outside this region the sensors measurements are zero. The measurements of the sensors were normalized to the maximum value according to the procedure described in the paper [17]. Fig. 8 presents a comparison of sensor measurements and its predicted values using the satellite motion model with initial conditions obtained using the magnetometer data. There is some correlation between the corresponding curves, but the discrepancy in the numerical values can be explained by the unaccounted influence of the Earth's albedo, which also affects the sun sensors measurements and its contribution can reach up to 30% of the Sun's influence. In particular, non-zero measurements from solar sensors № 5 and 6 can be explained by the effect of the light reflected from the Earth.

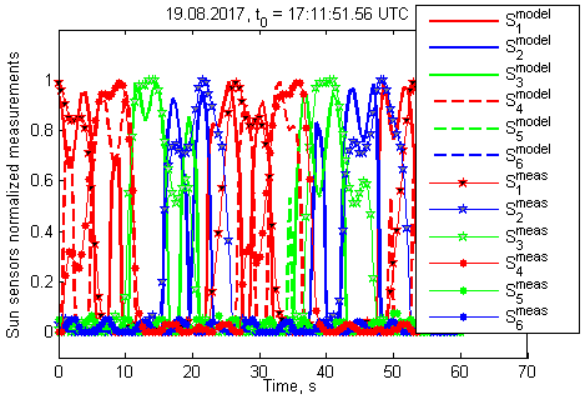

Fig. 8. Sun sensors normalized measurements and its predicted values

Fig. 9 shows the dependence of the angular velocity modulus on time after the launch of the satellite. The graph is close to linear, which corresponds to the damping model using hysteresis dampers. From the graph it can be concluded that it took about 36 days for damping and achieving a magnetic attitude, which is due to a high initial angular velocity of 79 deg/s.

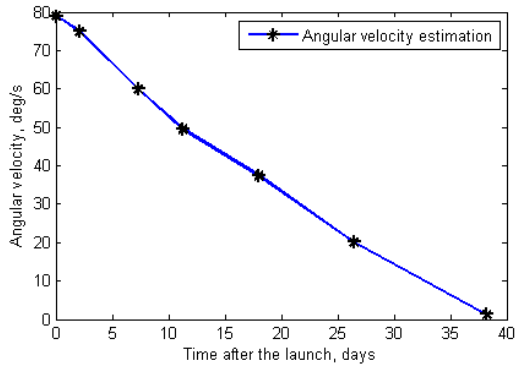

Fig. 9. Dynamics of angular velocity damping

4.2. Magnetic stabilization of TNS-0 # 2 nanosatellite

On October 2 it was possible to obtain telemetry recorded on the onboard storage in a time approximately equal to 2 orbits. The initial conditions for the motion model of the nanosatellite TNS-0 #2 were determined using the least squares method described above. Fig. 10 (a) shows a graph of the deviation angle of the OZ axis from the local magnetic field vector. It can be seen that this angle does not exceed 12 degrees, and the average deviation along the orbit is about 5 degrees. This graph can be considered almost classical. It clearly shows the characteristic period of the forced oscillations (about 9 minutes) caused by the uneven rotation of the local geomagnetic field induction vector. Its frequency is close to the frequency of the satellite's natural oscillations as a rigid body with a permanent magnet in a constant external magnetic field. The period of comparatively slow amplitude variation of these oscillations (a time equal to half the satellite's revolution in orbit around the Earth) is associated with a change in the magnitude of the induction vector of the local geomagnetic field. Fig. 10b is a graph of the angular velocity during the motion, which shows that the satellite continues to rotate about the longitudinal axis with an angular velocity of 0.4 deg/s, and two other axes oscillates.

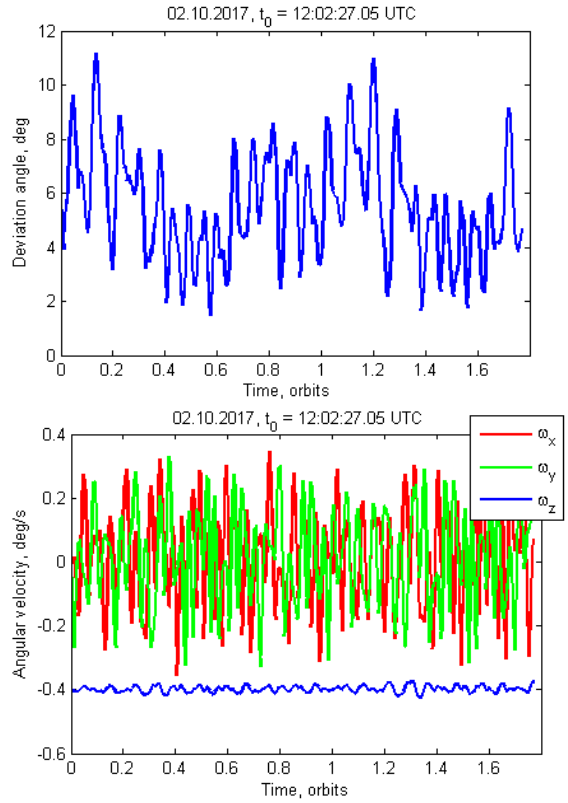

Fig. 10. Angle of deviation of the OZ axis of the satellite from the direction of the local magnetic field (a) and the angular velocity during steady-state motion (b)

Measurements from photodiode sun sensors were predicted based on the initial conditions obtained, and their values were compared with telemetry data. The result of the comparison is shown in Fig. 11. The measurement forecast coincides with some accuracy with the measurements of the photodiode sensors. It should be noted that a cosine-wave sensor measurement model was used for the prediction of measurements, which does not work well at large deviation angles, and the contribution from the Earth's albedo was not taken into account. The 5th and 6th solar sensors are located on the opposite sides of the satellite body. Therefore at the time when the measurements of the 5th sensor are close to unity, the measurements of the 6th sensor reaches 0.3 value, that can be caused only by the reflection of sunlight from the Earth. Thus, the fact is confirmed that the albedo of the Earth can be up to 30% of the solar radiation is confirmed.

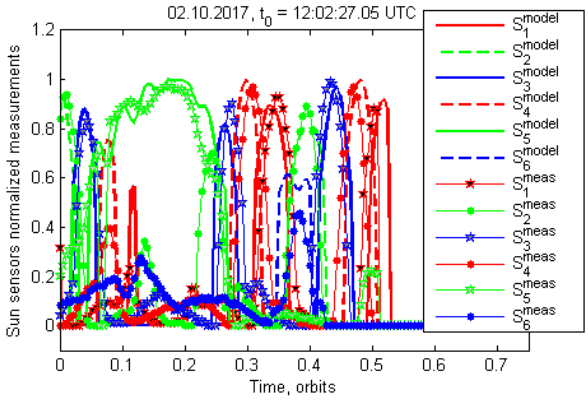

Fig. 11. Sun sensors normalized measurements and its predicted values

The TNS-0#2 satellite has passive magnetic stabilization since October 2017 till the last several months of the mission. The angle of the deviation of the magnetical axis relative to local geomagnetic filed direction for a set of months in 2018 year is shown in Fig. 12. The angle of deviation do not exceed 12 deg.

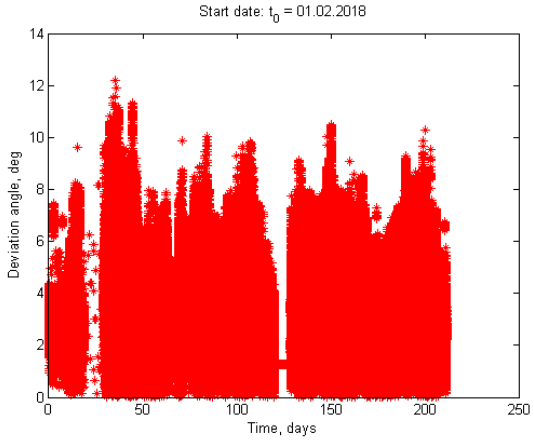

Fig. 12. Angle of deviation of the OZ axis of the satellite from the direction of the local magnetic field

With the orbit degradation the angle of the deviation gradually increased due to increasing influence of the aerodynamic torque. The orbit altitude for the whole mission is shown in Fig. 13. And the Fig. 14 shows the angle of magnet axis deviation from the local geomagnetic field during last months starting from 1 July 2019. In July 2019 the deviation was up to 40 deg and in August 2019 there was no magnetic stabilization and it seems that the satellite was tumbling. After 2 weeks we found out that the satellite achieved the aerodynamic stabilization – its axis of dynamical symmetry tracked the incoming airflow direction. And in the very last day of the mission 6 September the telemetry processing showed that the satellite lost the aerodynamic stabilization.

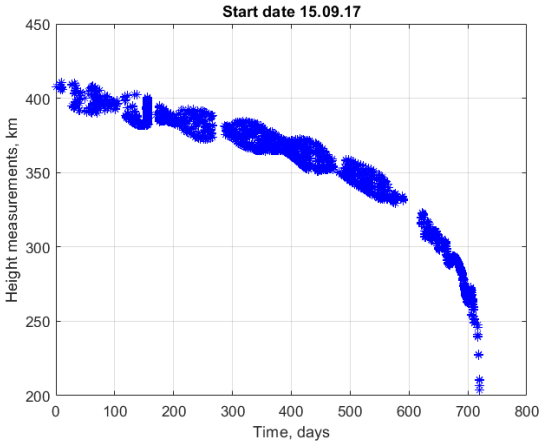

Fig. 13. Altitude calculated using measurements from onboard GPS/GLONASS receiver

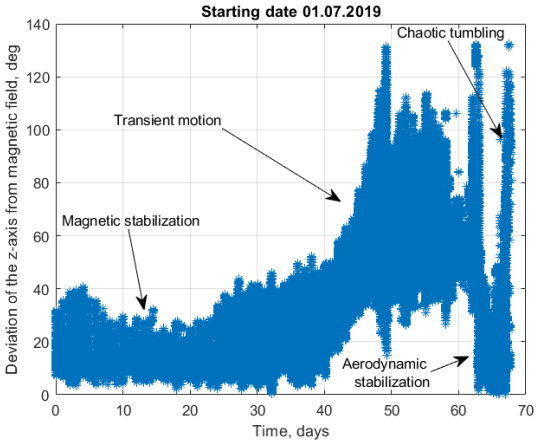

Fig. 14. Angle of deviation of the OZ axis of the satellite from the direction of the local magnetic field

Consider in details the attitude motion regimes during the last month of the satellite mission in the following sections.

4.3 Transient attitude motion

Consider measurements obtained from the telemetry at 20th August 2019. The satellite altitude was 240 km, the average atmosphere density value is $4 \cdot 10^{-11}$ kg/m^3. With this density the value of the atmosphere dencity the aerodynamic torque is of the same order with the magnetic torque. To estimate the shift of the center of pressue relative to the center of mass we included this parameter to the vector of unknown parameters and obtained that the displacement is about 7 cm along the axis of dynamical symmetry. After processing of obtained measurements using the described technique it is obtained that the satellite lost the magnetic stabilization, the angle if the magnet axis and the local magnetic field reaches almost 75 deg as can be seen

from Fig. 15. However, the aerodynamical stabilization is not yet achieved as can be concluded from Fig. 16, where the deviation of the axis of the dynamical symmetry from the direction of the incoming airflow is shown. The satellite is in the transient motion and its angular motion is up to 3 deg/s as can be seen from Fig. 17.

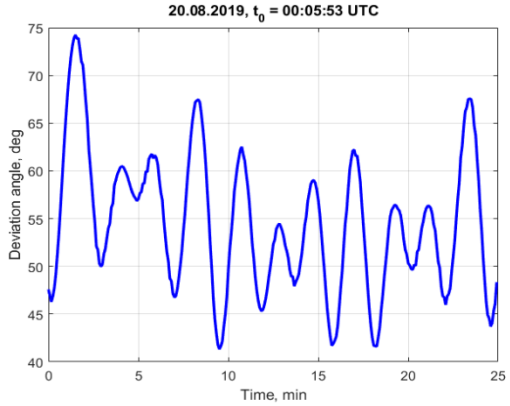

Fig. 15. Angle of deviation of the OZ axis of the satellite from the direction of the local magnetic field

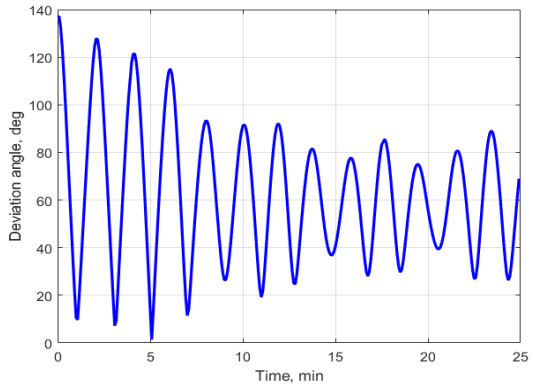

Fig. 16. Angle of deviation of the OZ axis of the satellite from the direction of incoming air flow

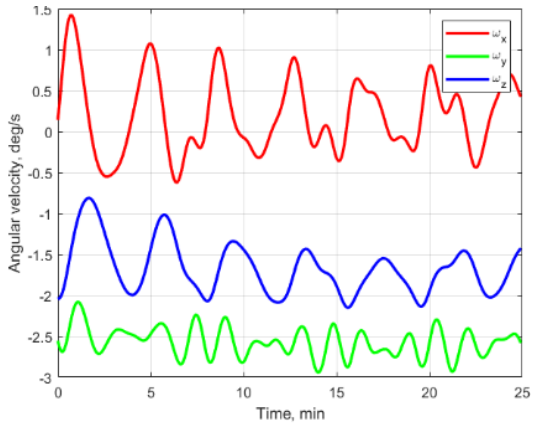

Fig. 17. Estimated angular velocity

4.4 Aerodynamic attitude stabilization

The tumbling attitude motion was gradually transited during 2 weeks to stabilized satellite motion. The onboard hysteresis rods damped the angular motion of during the tumbling. Consider the results of the telemetry processing obtained 5th September 2019. The altitude is 180 km and the atmosphere density is $3 \cdot 10^{-10}$ kg/m^3. The aerodynamic torque is an order of magnitude greater than the magnetic torque. The deviation of the axis of the dynamical symmetry from the direction of the incoming airflow does not exceed 30 deg according to the Fig. 18, the period of oscillations are about 2 min. The angular velocity decreased up to 0.5 deg/s (Fig. 19) and a slow permanent rotation along the OZ axis is observed as can be seen from Fig. 20.

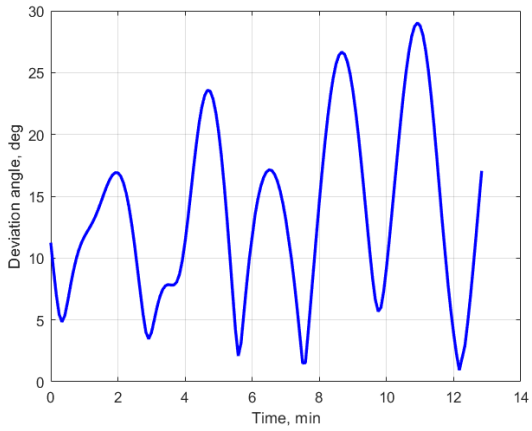

Fig. 18. Angle of deviation of the OZ axis of the satellite from the direction of incoming air flow

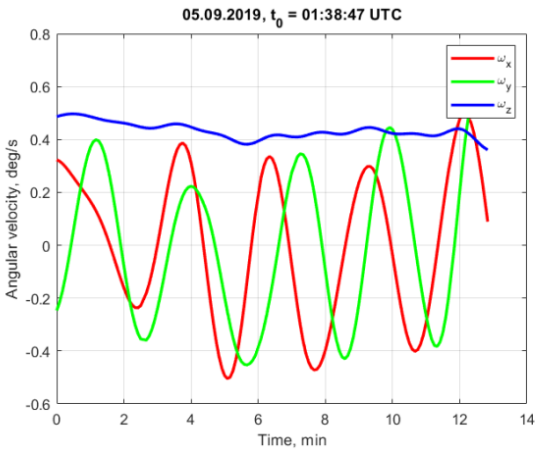

Fig. 19. Angular velocity in the body reference frame

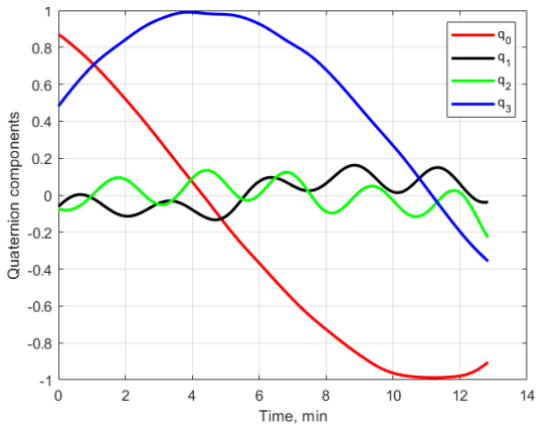

Fig. 20. Attitude quaternion

4.5 Tumbling during the very last day

It is interesting that during the very last day of the mission, on the 6th September 2019 when the altitude was of 153 km and the atmosphere density of $1.5 \cdot 10^{-9}$ kg/m^3 the satellite lost the aerodynamic stabilization probably due to turbulent effect. The last received data was processed and it was found out that the deviation of the axis of dynamical symmetry relative to the incoming airflow is up to 100 deg and angular velocity is about 5 deg/s as can be seen from Fig. 21 and Fig. 22.

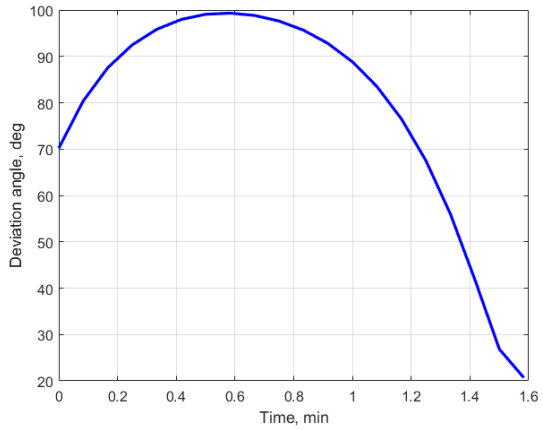

Fig. 21. Angle of deviation of the OZ axis of the satellite from the direction of incoming air flow

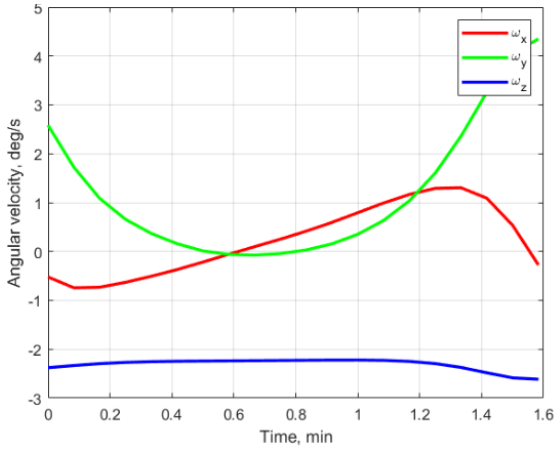

Fig. 22. Angular velocity in the body reference frame

Conclusions

The attitude motion of the TNS-0 #2 satellite during the last month of the mission is analyzed. It is shown that with orbit altitude decay the aerodynamic torque gradually prevailed over the magnetic torque that caused the transition from the passive magnetic stabilization of the about 12 deg of accuracy to the passive aerodynamic stabilization with deviation from the incoming airflow of about 30 deg. The communication via GlobalStar allowed to obtain enough onboard sensor measurements to reconstruct the attitude motion even during the extremely low flight with altitude of 153 km, probably just before the breakdown of the satellite in the dense atmospheric layers.

Acknowledgements

The work is supported by Russian Science Foundation, grant 17-71-20117.

References

[1] M. Ovchinnikov, D. Ivanov, O. Pansyrnyi, A. Sergeev, I. Fedorov, A. Selivanov, O. Khromov, N. Yudanov, Technological NanoSatellite TNS-0 #2 Connected Via Global Communication System, Acta Astronautica. 170 (2020) 1–5. doi:10.1016/j.actaastro.2020.01.027.

[2] V.A. Sarychev, M.Y. Ovchinnikov, Satellite Magnetic Attitude Control Systems, Itogi Nauk, VINITI, Moscow, 1985.

[3] V.A. Sarychev, M.Y. Ovchinnikov, Attitude magnetic stabilization using spherical damper, Cosmic Research. 24 (1986) 803–815.

[4] V.A. Sarychev, M.Y. Ovchinnikov, Attitude motion of the satellite with permanent magnet, Cosmic Research. 24 (1986) 527–543.

[5] V.A. Sarychev, V.V. Sazonov, Estimation of the infuence from the eddy-current on the fast satellite rotation, Cosmic Research. 2 (1982) 297–300.

[6] V.A. Sarychev, V.V. Sazonov, Optimal parameters of the passive magnetic attitude control systems, Cosmic Research. 14 (1976) 198–208.

[7] M.L. Battagliere, F. Santoni, M. Ovchinnikov, F. Graziani, Hysteresis rods in the passive magnetic stabilization system for university micro and nanosatellites, in: Proceedings of the 59th IAC, Glasgow, UK, 29 September–3 October, Paper IAC-08.C.1.8, 2008: p. 10.

[8] M. Long, A. Lorenz, G. Rodgers, E. Tapio, G. Tran, K. Jackson, R. Twiggs, T. Bleier, A Cubesat Derived Design for a Unique Academic Research Mission in Earthquake Signature Detection, in: 16th Annual/USU Conference on Small Satellites, Logan, Utah US, 12-15 August, 2002, Paper SSC02-IX-6, n.d.: p. 17.

[9] Y. Tsuda, N. Sako, T. Eishima, T. Ito, Y. Arikawa, N. Miyamura, A. Tanaka, S. Nakasuka, University of Tokyo's CubeSat Project - Its Educational and Technological Significance, in: 15th Annual AIAA/USU Conference on Small Satellites, Logan, Utah, 13 – 16 August, 2001, Paper SSC01-VIIIb-7, n.d.: p. 8.

[10] M.L. Battagliere, F. Santoni, F. Piergentili, M. Ovchinnikov, F. Graziani, Passive magnetic attitude stabilization system of the EduSAT microsatellite, Aerospace Engineering. 224 (2010) 1097–1107.

[11] F.T. Hennepe, B.T.C. Zandbergen, R.J. Hamann, Simulation of the Attitude Behaviour and Available Power Profile of the Delfi-C3 Spacecraft with Application of the OpSim Platform, in: Paper at the 1st CEAS European Air and Space Conference, Berlin, Germany, 10-13 September 2007, n.d.: p. 9.

[12] M.Y. Ovchinnikov, D.S. Ivanov, N. a. Ivlev, S.O. Karpenko, D.S. Roldugin, S.S. Tkachev, Development, integrated investigation, laboratory and in-flight testing of Chibis-M microsatellite ADCS, Acta Astronautica. 93 (2014) 23–33. doi:10.1016/j.actaastro.2013.06.030.

[13] D. Ivanov, M. Ovchinnikov, N. Ivlev, S. Karpenko, Analytical study of microsatellite attitude determination algorithms, Acta Astronautica. 116 (2015) 339–348. doi:10.1016/j.actaastro.2015.07.001.

[14] T. Beuselinck, C. Van Bavinchove, V.I. Abrashkin, A.E. Kazakova, V. V. Sazonov, Determination of attitude motion of the Foton M-3 satellite according to the data of onboard measurements of the Earth's magnetic field, Cosmic Research. 48 (2010) 246–259. doi:10.1134/S0010952510030068.

[15] V.I. Abrashkin, K.E. Voronov, Y.Y. Piyakov, V.V. Sazonov, N.D. Semkin, S.Y. Chebukov, Attitude motion of the Photon M-4 satellite, Cosmic Research. 54 (2014) 315–322. doi:10.7868/S0023420616040014.

[16] V.I. Abrashkin, K.E. Voronov, I. V. Piyakov, Y.Y. Puzin, V. V. Sazonov, N.D. Semkin, S.Y. Chebukov, Rotational motion of Foton M-4, Cosmic Research. 54 (2016) 296–302. doi:10.1134/S0010952516040018.

[17] D.S. Ivanov, M.Y. Ovchinnikov, O.A. Pantsyrnyi, A.S. Selivanov, A.S. Sergeev, I.O. Fedorov, O.E. Khromov, N.A. Yudanov, Nanosatellite TNS-0 №2 Attitude Motion After The Launch From ISS, Cosmic Research. 57 (2019) 272–288. doi:10.1134/S0010952519040038.

[18] V.A. Sarychev, V.I. Penkov, M.Y. Ovchinnikov, Mathematical model of hysteresis based on magneto-mechanical analogy, Mathematical Simulation. 1 (1989) 122–133.

[19] D. Ivanov, M. Ovchinnikov, M. Sakovich, Relative Pose and Inertia Determination of Unknown Satellite Using Monocular Vision, International Journal of Aerospace Engineering. (2018) 1–16. doi:10.1155/2018/9731512.